Bulk microstructure evolution of two high Hf-containing Ni-based alloys during exposure at temperatures from 1100 to 1250°C

Patrice Berthod, Dame Assane Kane

Research Article

Chemical Review and Letters
journal homepage: www.chemrevlett.com
ISSN (online): 2645-4947 (print) 2676-7279

Bulk microstructure evolution of two high Hf–containing Ni–based alloys during exposure at temperatures from 1100 to 1250°C

Patrice Berthod[a,b] ∗, Dame Assane Kane[b]

[a]*Université de Lorraine, CNRS, IJL, Nancy, France*
[a]*Université de Lorraine, FST, Vandoeuvre–lès-Nancy, France*

ARTICLE INFO

Article history:
Received 9 January 2021
Received in revised form 25 January 2021
Accepted 26 January 2021
Available online 27 January 2021

Keywords:
Nickel-based alloy
High Hf content
High temperature exposure
Metallographic characterization
Hardness

ABSTRACT

Two Hf–poorest versions of a high performance chromia–forming nickel–based polycrystalline cast alloy reinforced by HfC carbides were investigated by replacing more or less hafnium by tantalum to reduce production cost. After elaboration, microstructure control, thermal analysis and exposures at temperature were carried out on samples cut in the obtained ingots. The as–cast microstructures of the two alloys are similar to the initial alloy one but their behaviors at the three considered high temperatures (1100, 1200 and 1250°C) were more or less different: more fragmentation of the MC carbides and precipitation of chromium carbides during aging. Some decreasing effects on the room temperature hardness were observed, and one can suppose that the high temperature mechanical properties of these two {(Hf,Ta)C carbides}–containing alloys derived from the HfC–strengthened initial one may be lowered.

1. Introduction

Except some alloys based on very refractory metals such as molybdenum, tungsten or tantalum [1, 2], materials for uses at very high temperatures are more often ceramic than metallic. Alumina–based ceramics, molybdenum silicides, silicon nitrides or silicon carbides are among the most popular structural ceramics. Other ceramic materials, composed of SiC [3–6], Si_3N_4 [7], $TaSi_2$ [8], ZrB_2 [9, 10] or MoB [11] with HfB_2 also exist as well as other ones based on HfB_2 [11–13]. In addition to HfB_2 borides, HfO_2 oxides [14, 15], $HfSi_2$ silicides [16], HfN nitrides [17] and HfC carbides [18–23] are also species involving hafnium which are used in ceramic materials for ultra–high temperatures. Such ceramic materials are very refractory and resistant against the chemical aggressiveness of the hot environment to which they can be exposed in service, but the main problem is their lack of ductility and of toughness that may cause brittle failures.

Metallic alloys may better resistance against crack propagation due to their much better ductility. Their mechanical resistance at elevated temperature may be of a reasonable level when they are efficiently strengthened by hard particles present in sufficiently high quantities. MC monocarbides feature in good position thank to their distribution and their morphologies in alloys elaborated by casting, and here too hafnium owns a particularly important potential when it is present in the composition of MC carbides.

Rather high volume fractions of HfC carbides were successfully obtained in metallic alloys based on cobalt, nickel or iron [24–26], with potentially good effect on the mechanical properties at high temperatures but by preserving toughness and ductility. More, the high morphological stability of these carbides allows envisaging to use the best ones of these alloys – the ones based on cobalt, eventually on nickel – at very high temperatures (may be up to 1300°C) under low applied stresses, in competition with the less refractory of the ceramic materials cited above. Unfortunately, due to the high contents of the expensive Hf element, such alloys may be a little too costly. To reduce their cost of production it can be thought to substitute more or less hafnium by another MC–forming element, tantalum. This was tested in this work, by choosing two compositions

∗ Corresponding author. Tel.: +33372742729; Fax: +33372742401; e-mail: patrice.berthod@univ-lorraine.fr

and by elaborating the corresponding alloys. The microstructures of the two alloys after fabrication were investigated to compare the morphologies of the obtained carbides to the ones of HfC carbides previously obtained in similar alloys. These alloys were also exposed to high temperatures of different levels to study how may evolve their microstructure and their hardness after return to room temperature.

2. Experimental

2.1. Fabrication of the alloys

Two alloys were cast for the study. Their compositions (in wt.%) are Ni(bal.)–25Cr–0.4C–2Ta–4Hf (named "***tH***") and Ni(bal.)–25Cr–0.4C–4Ta–2Hf (named "***Th***"). A high frequency induction furnace (CELES) was used. Pure elements (Alfa Aesar, purity > 99.9%) were initially placed in the copper crucible of the furnace. The melting chamber was closed with a silica tube and an internal inert atmosphere of 400mbars of pure argon was created inside).

Melting was achieved by generating an alternative electrical current (frequency: 110 kHz, voltage: increase from 0 to 5kV (and maintained at 5kV for 5 min) for heating and melting, and return to 0 for solidification and cooling. The two obtained ingots, both weighing about 40 grams, were geometrically ovoid.

2.2. Determination of the melting ranges of the two alloys

Before deciding the temperatures of the heat exposures, the two alloys were subjected to Differential Thermal Analysis/DTA. In each ingot a 2 × 2 × 7 mm^3 parallelepiped was cut in the ingot, and was placed in a small cylindrical alumina crucible. The crucible containing the alloy parallelepiped was placed in the hot zone of a SETARAM TG–ATD machine where it was subjected to a heating at +20°C / min up to 1200°C, and at +5°C / min thereafter up to 1500°C. Cooling was then applied with first -5°C / min down to 1200°C then -20°C / min down to room temperature. The heat exchanges between the alloy sample and the machine were recorded, in order to be able to plot the thermal flow versus temperature.

2.3. Exposures to high temperatures

Each ingot was cut to obtain four parallelepipeds prepared for the initial microstructure control and for the high temperature exposures: one 5 × 5 × 5 mm^3 (as–cast microstructure characterization) and three 3 × 10 × 10 mm^3 (exposures at high temperature); the three last ones were additionally ground with 1200grit SiC papers on their two main square faces and on their four smaller rectangular faces, with smoothing of edges and corners to avoid any overoxidation followed by possible oxidation–induced destruction.

The three samples destined to high temperature exposures were exposed in a tubular resistive furnace for 50 hours in air: one at 1100°C, one at 1200°C and one at 1250°C. The heating and cooling rates were respectively 20°C / min and -5°C / min in all cases.

2.4. Microstructure characterization and indentation tests

The as–cast part and the three samples aged at high temperature (each cut in two parts) were embedded in a resin system rigidifying at low temperature (mix of resin and hardener, ESCIL), then ground (SiC papers from 240grit to 1200grit), washed (ultrasounds in water) and polished (3 µm hard particles on textile disk). The as–cast or aged microstructures of the obtained mirror–like samples were then observed by electron microscopy (scanning electron microscope/SEM in back scattered electrons mode/BSE under 20kV of acceleration voltage). The alloy chemical compositions were controlled by energy dispersive spectrometry/EDS using the corresponding device attached to the SEM (JEOL JSM 6010LA). The chemical compositions of the matrix and of second phases were measured by spot EDS analysis.

The hardness of both alloys for the four different states (as–cast and aged at the three temperatures) were determined by Vickers indentation under 10kg–load, using a Testwell apparatus.

3. Results and Discussion

3.1. As–cast microstructures

The microstructures of the two alloys are illustrated by SEM/BSE micrographs, taken at medium magnification, in Figure 1 (***tH*** alloy) and in Figure 2 (***Th*** alloy). Both alloys, just after casting, are composed of a matrix and of carbides. In the two alloys the matrix is dendritic. It was certainly the first solid phase to precipitate during solidification. The carbides, located ate the interdendritic boundaries, crystallized at the end of solidification, during a eutectic reaction. Indeed they are closely mixed with the peripherical part of the dendrites, which leads thinking that they precipitated from the residual liquid according to the global transformation {liquid → matrix + carbide}.

In the case of the ***tH*** alloy, there is a single eutectic: matrix + MC carbide (brighter than matrix), while there are obviously two eutectics in the case of the ***Th*** alloy: matrix + MC carbide (brighter than matrix, Chinese script morphology) and matrix + chromium carbide (darker than matrix, acicular morphology). Indeed, spot EDS analysis performed on the coarsest ones among the carbides of the two types demonstrated clearly that the bright carbides are rich in C, Hf and Ta while the dark/black carbides are rich in C and Cr. More precisely, the MC carbides are seemingly of the $(Hf_{0.67},Ta_{0.33})C$ stoichiometry in the ***tH*** alloy and of the $(Hf_{0.5},Ta_{0.5})C$ stoichiometry in the ***Th*** alloy. The chromium carbides, present in ***Th*** alloy, are seemingly Cr_7C_3 carbides.

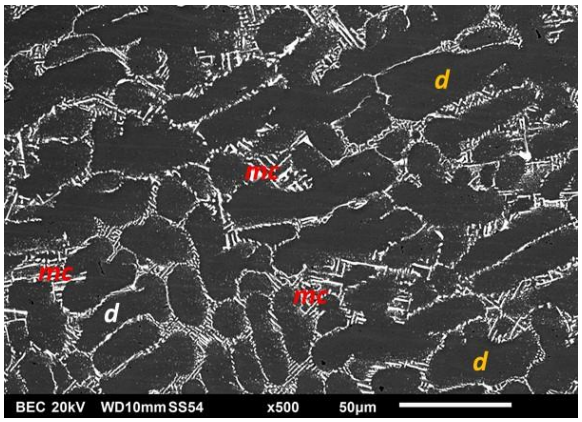

Figure 1. The as–cast microstructure of the ***tH*** alloy (SEM/BSE micrograph); gray dendritic Ni–based matrix (***d***) and bright script–like (Hf,Ta)C eutectic carbides (***mc***)

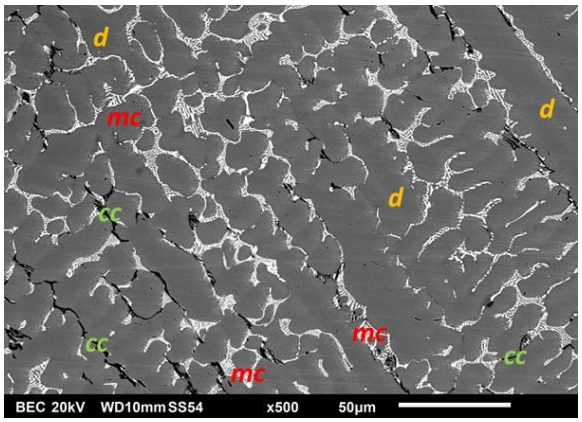

Figure 2. The as–cast microstructure of the ***Th*** alloy (SEM/BSE micrograph); gray dendritic Ni–based matrix (***d***), bright script–like (Hf,Ta)C eutectic carbides (***mc***) and black acicular Cr_7C_3 eutectic carbides (***cc***)

Additionally, the chemical compositions of the two alloys were measured by full frame EDS analysis on several ×250 areas. The results showed targeted contents in Cr, Ta and Hf were well respected, however a little overestimated in the cases of tantalum and hafnium (a classical consequence of the presence of these elements mainly with the form of rather coarse carbides). The content in carbon, which is not measurable by EDS by full frame analysis of alloys rather low in this light element, was however considered as well respected by looking to the densities of the obtained carbides networks (typical of 0.4 or 0.5 wt.%C).

3.2. DTA experiments

The obtained {thermal flow versus temperature} curves are plotted in Figure 3 for the ***tH*** alloy and in Figure 4 for the ***Th*** alloy. Seemingly the melting of ***tH*** alloy (red curve) was realized in two successive steps, as well as its re–solidification. The low temperature peak at heating and the low temperature peak at cooling can be interpreted as the melting and the solidification of the {MC carbides + matrix} eutectic compound, while the high temperature peaks at heating and at cooling correspond respectively to the melting and to the crystallization of the matrix dendrites. The heating and cooling curves recorded for the ***Th*** alloy are a little more complex. Obviously this results from the melting of the two eutectics occurring with a small gap which led to overlapping. The same can be said concerning the solidification of the two eutectics.

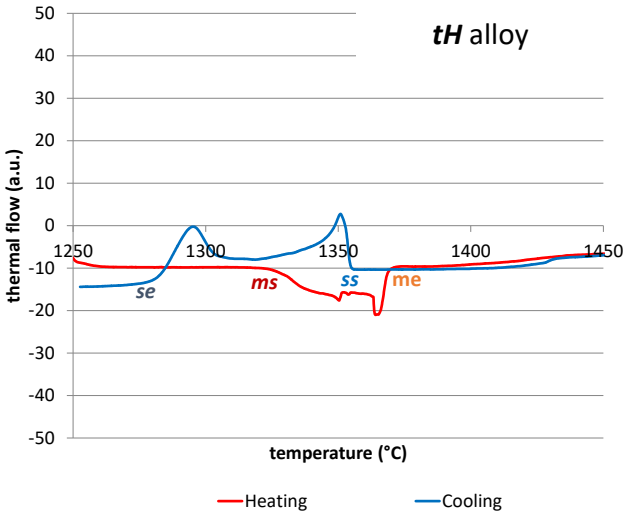

Figure 3. Differential scanning calorimetry run carried out on the ***tH*** alloy; heating part: melting start (***ms***), melting end (***me***); cooling part: solidification start (***ss***) and solidification end (***se***)

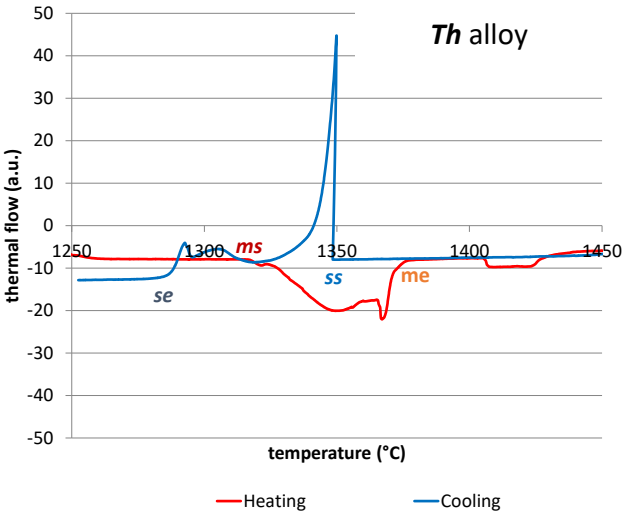

Figure 4. Differential scanning calorimetry run carried out on the ***Th*** alloy; heating part: melting start (***ms***), melting end (***me***); cooling part: solidification start (***ss***) and solidification end (***se***)

Attention was particularly focused on the temperatures of start of melting and of solidification's end, in order to define a maximal temperature for the exposures to heat. Taking into account the obtained values (all ≥ 1280°C, Table 1), it was decided to limit the test temperature at 1250°C, temperature at which it is still sure that both alloys are wholly solid. So, the exposures to heat were driven at 1250°C, 1200°C and 1100°C, temperature far enough to one another and high enough to represent the service temperature levels which may concern such particular alloys rich in Hf to stabilize the reinforcing carbides.

Table 1. Exploitation of the DTA curves

Temperatures of	***tH* alloy**	***Th* alloy**
Melting start	1317 °C	1318 °C
Melting end	1373 °C	1378 °C
Solidification start	1357 °C	1349 °C
Solidification end	1280 °C	1284 °C
Liquidus (estimated)	1365°C	1364°C
Solidus (estimated)	1299°C	1301°C

*3.3. Microstructures of the **tH** alloy after 50 hours at 1100, 1200 or 1250°C*

After 50 hours spent at 1100°C, 1200°C and 1250°C, the bulk microstructure of the ***tH*** alloy has evolved more or less, as illustrated in Figures 5–7. After exposure at 1100°C the microstructure stayed almost unchanged, except the discrete precipitation of small dark chromium carbides close to the interdendritic boundaries (Figure 5).

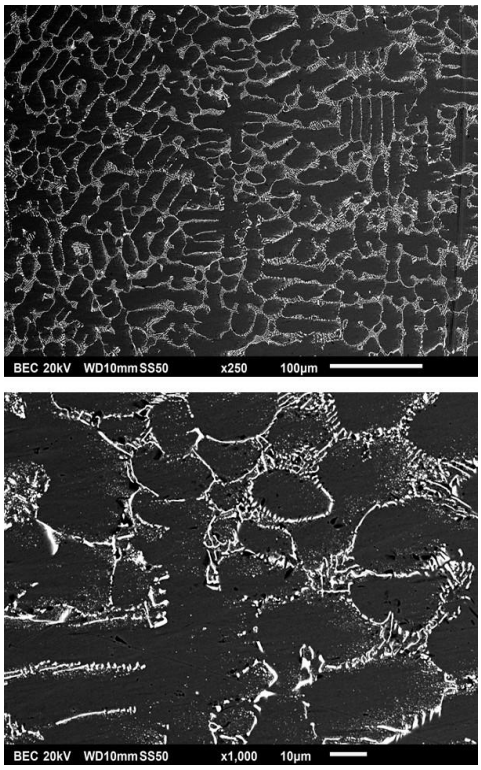

Figure 5. The microstructure of the ***tH*** alloy after 50h at 1100°C (SEM/BSE micrograph)

50 hours at 1200°C did not modify considerably the microstructure of the alloy (Figure 6). However two minor changes are to be noted. First, the secondary MC carbides which were initially present in the neighborhood of the interdendritic spaces, and which were still here after the 1100°C exposure, have totally disappeared. Second, as after 50h at 1100°C, additional chromium carbides have precipitated and seem to be a little more numerous and significantly coarser than for 1100°C.

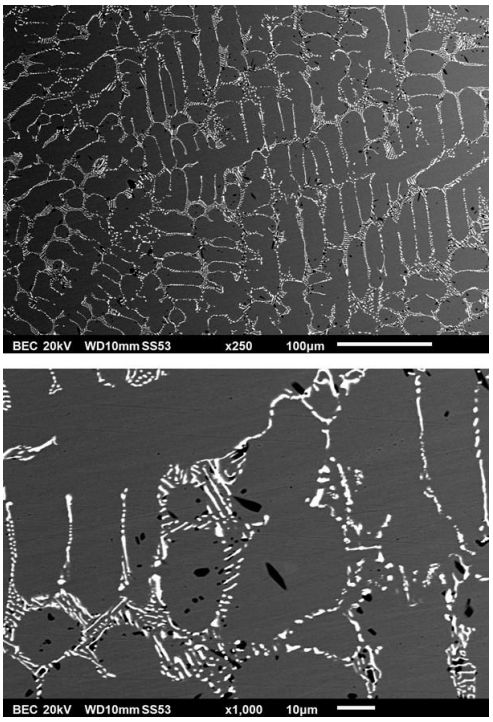

Figure 6. The microstructure of the ***tH*** alloy after 50h at 1200°C (SEM/BSE micrograph)

Unsurprisingly, this is for 1200°C that the microstructure of the ***tH*** alloy has evolved the most (Figure 7). Some of the chromium carbides are much coarser than for the two previous stage temperatures, and the MC carbides are fragmented. All of the initial script–like shaped MC carbides are converted into alignments of globular MC carbides.

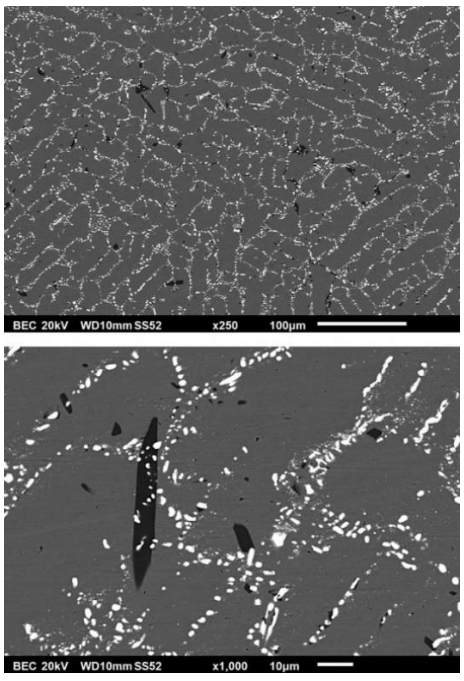

Figure 7. The microstructure of the ***tH*** alloy after 50h at 1250°C (SEM/BSE micrograph)

*3.4. Microstructures of the **Th** alloy after 50 hours at 1100, 1200 or 1250°C*

The ***Th*** alloy was affected by similar phenomena during its stages at high temperature, except the secondary precipitation of MC carbides occurred at 1100°C at the dendrites boundaries. Indeed, at 1100°C (Figure 8) small MC precipitated in these areas where no such fine carbides were initially present, but the coarsening of the chromium carbides (initially present in the as–cast state in the case of this alloy) is more and more in progress for stage temperature higher and higher. After 50 hours at 1200°C the script–like shape of the MC carbides is already affected (Figure 9) and for 1250°C too (Figure 10), MC fragmentation is more advanced than for the first alloy.

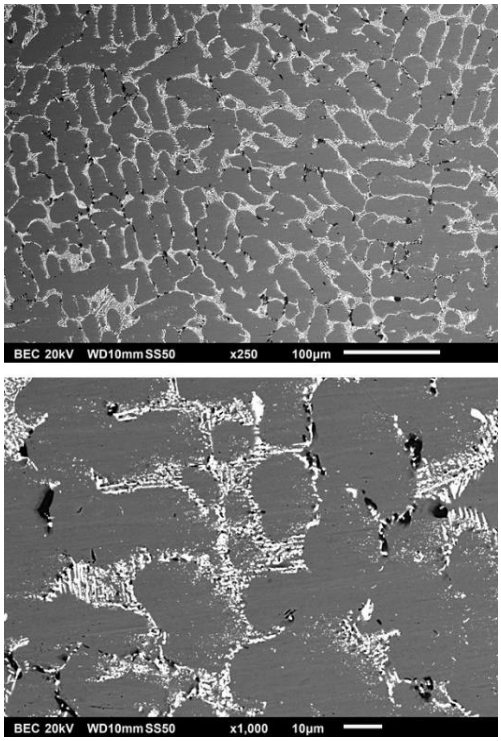

Figure 8. The microstructure of the ***Th*** alloy after 50h at 1100°C (SEM/BSE micrograph)

3.5. Quantitative data concerning the microstructure changes: chemical composition of the matrix

During the microstructure observations above, not only changes in morphology were noticed, but it also seemed that the surface fractions of the two types of carbides may have evolved during the high temperature exposures. Image analysis is possible to estimate these surface fractions since the three present phases are of gray levels rather different. It was preferred here to determine these surface fractions by using an indirect way: the mass fractions of the MC carbides were deduced from the difference in Hf and Ta contents between the whole alloy and the matrix. The weight fractions of carbides were thus deduced and converted in volume fraction using the volume masses of matrix and MC carbides. To allow doing that it is preliminarily compulsory to measure the chemical compositions of the matrixes of the two alloys and for their as–cast states and their three high temperature aged states. This was done by EDS spot analysis in matrix, performed five times in various locations. The calculated average and standard deviation values are graphically represented in Figure 11 for the ***tH*** alloy and in Figure 12 for the ***Th*** alloy. One can see first that the chromium content in matrix slightly increases for both alloys, from the as–cast state to the 1100°C–aged state, and among the aged–states, it increases slightly with the aging temperature exclusively for the ***tH*** alloy.

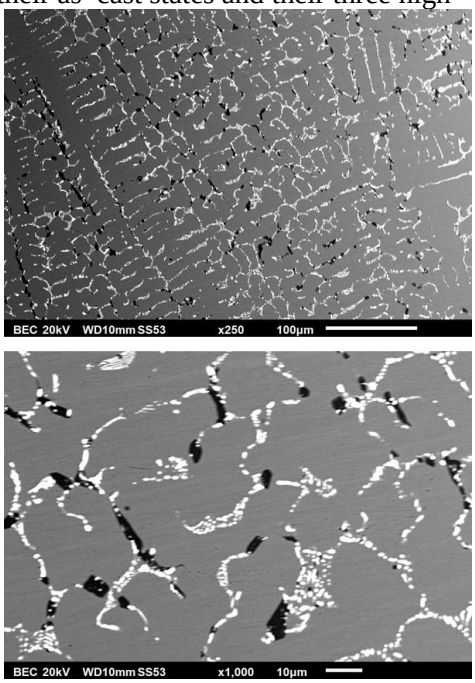

Figure 9. The microstructure of the ***Th*** alloy after 50h at 1200°C (SEM/BSE micrograph)

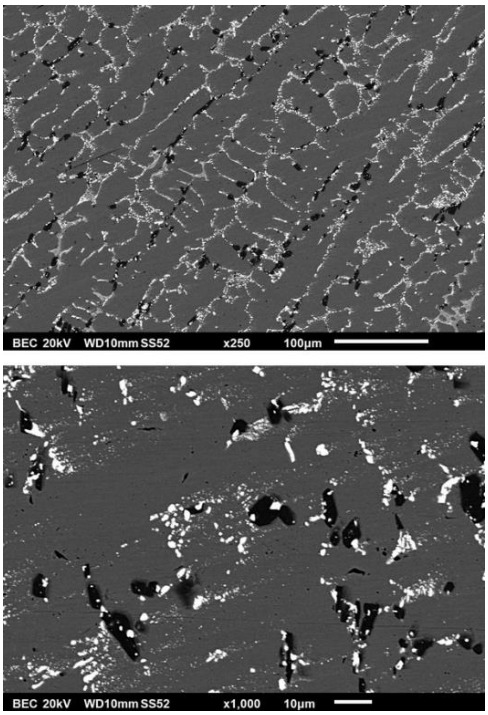

Figure 10. The microstructure of the ***Th*** alloy after 50h at 1250°C (SEM/BSE micrograph)

Concerning tantalum, an obvious decrease in content can be observed from the as–cast state and the 1100°C–aged state. It seems that this decrease goes on when the aging temperature increases.

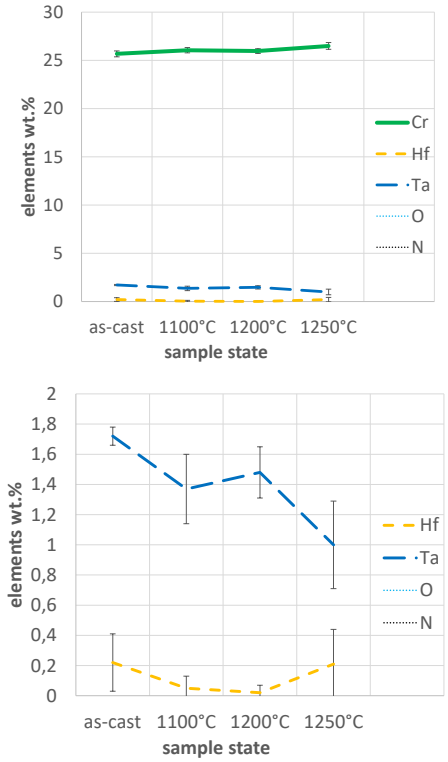

Figure 11. The minor elements contents in matrix for the four different metallurgical states of ***tH*** alloy (top: all elements, bottom: Cr excluded)

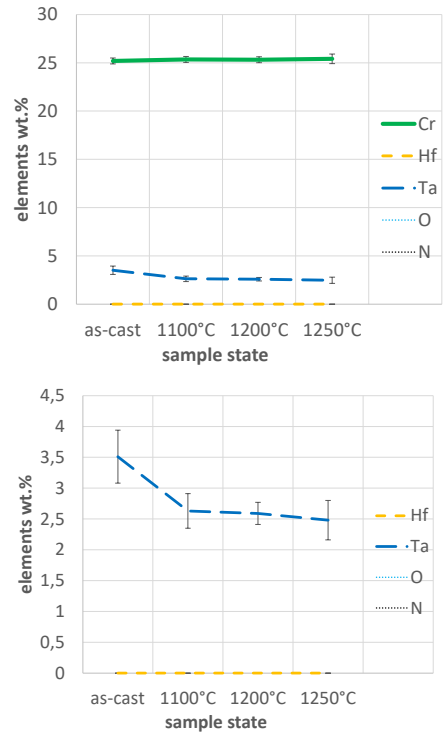

Figure 12. The minor elements contents in matrix for the four different metallurgical states of ***Th*** alloy (top: all elements, bottom: Cr excluded)

3.6. Quantitative data concerning the microstructure changes: mass fractions and volume fractions

The differences in Hf and Ta contents between alloy and its matrix were exploited according to a method previously described [27] in order to estimate the mass fractions (Figure 13) and volume fractions (Figure 14) of MC carbides. In both figures, the average mass fractions and volume fractions coming from the average Hf+Ta weight content differences are graphically given ± one standard deviation. For both alloys the mass fraction in MC carbides in the three aged states are higher than for the as–cast state, this meaning that the exposures at high temperature allowed finishing precipitating MC carbides. The mass fractions obtained after the exposures at high temperature are not significanltly dependent on the stage temperature. Globally, the ***tH*** alloy contains about 2.8 mass.%MC in the as–cast state and 3.7 mass%MC after aging, whatever the temperature. In the same time, the ***Th*** alloy contains about 4.3 mass.%MC in its as–cast state and around 5.0 mass.% after aging.

After conversion in volume fractions, these numbers become, in vol.%, about 1.9 (***Th*** alloy) and 3.1 (***tH*** alloy) for the as–cast states, and 2.7 (***Th*** alloy) and 3.4 (***tH*** alloy) for the high temperature aged states.

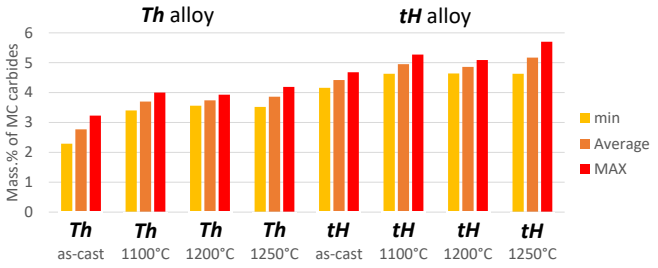

Figure 13. The mass fractions of (Ta,Hf)C carbides for the ***Th*** (lowest fractions) and ***tH*** (highest fractions) alloys for the four metallurgical states

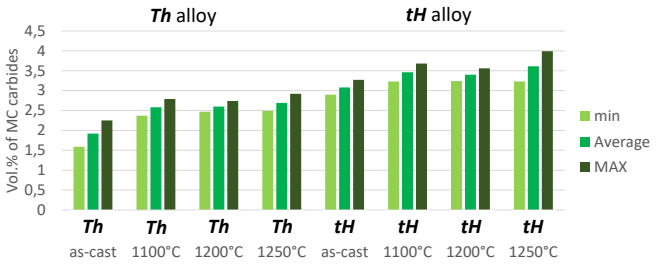

Figure 14. The volume fractions of (Ta,Hf)C carbides for the ***Th*** (lowest fractions) and ***tH*** (highest fractions) alloys for the four metallurgical states

3.7. Hardness values

Vickers indentation was performed on the two alloys in their four states. The obtained average and standard deviation values are graphically presented in Figure 15 for the ***tH*** alloy and in Figure 16 for the ***Th*** alloy. Clearly, the ***tH*** alloy is harder than the ***Th*** one state by state: about 215Hv_{10kg} against 205Hv_{10kg} in the as–cast state, 195Hv_{10kg} against 185Hv_{10kg} in the 1100°C–aged and 1200°C–aged state. This is only in the 1250°C–aged state

that the ***Th*** alloy seems to be slightly harder than the ***tH*** alloy (but about 180Hv_{10kg} for both of them).

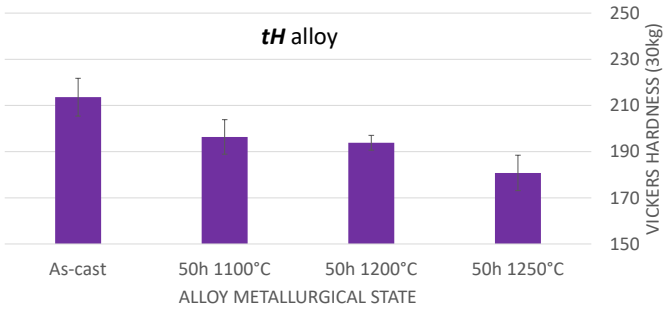

Figure 15. Evolution of the hardness of the ***tH*** alloy with the aging temperature

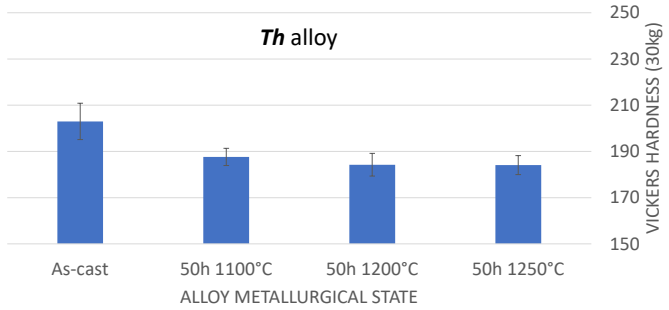

Figure 16. Evolution of the hardness of the ***Th*** alloy with the aging temperature

3.8. Some comments

Despite the less or more extended replacement of Hf by Ta, the as–cast microstructures of these Ni–based {25 wt.%Cr, 0.4wt.%}–containing alloys stay similar to a reference Ni (bal.)–based 25 or 30Cr–0.4 or 0.5C–5 to 6Hf (wt.%) alloy elaborated using the same apparatus and following the same procedure [26]. The microstructure of the as–cast ***tH*** alloy is almost identical to the reference alloy and its microstructure behavior at high temperature is almost the same, at least at 1100 and 1200°C. Indeed, the script–like morphology of the MC carbide is kept (no fragmentation), without decrease in volume fraction (this is curiously the inverse phenomenon that took place). This bodes well for the mechanical strength at elevated temperature. The single difference of microstructure behavior at high temperature between the ***tH*** alloy and the reference alloy is the solid state precipitation of chromium carbides in the alloy studied here. The ***Th*** alloy presented a microstructure a little different in the as–cast state (presence of small chromium carbides) and a microstructure behavior at 1100°C similar to the ***tH*** alloy's one. In contrast, its carbide network evolved significantly at higher temperature, even at 1200°C (MC fragmentation), temperature at which the Chinese script shape MC carbides of the ***tH*** alloy stayed unaffected. At 1250°C the MC carbides of both alloys were fragmented, but more for the ***Th*** alloy than for the ***tH*** one. It is clear that the ***Th*** alloy is less suitable for service at very high temperature than the ***tH*** one. Uses of the ***Th*** alloy seems to be limited at 1100°C while the ***tH*** alloy may be used at temperatures as high as 1200°C (temperature about one hundred degree below its melting start point).

With Vickers hardness lower than 220 Kv_{10kg}, the two alloys seem staying easy to machine, despite the their rather extended carbide networks in their as–cast states. This interesting property is to be attributed to the nickel–based matrix. For script–like shapes (as–cast microstructures in both cases) the ***tH*** alloy is harder than the ***hT*** alloy, probably because the first one contain more MC carbides. However, the dependence of the hardness on the microstructure is not so easy to understand since, in the aged–states, hardness is lower in both cases although the carbides quantity is higher than in the as–cast state. This may be attributed to the more or less advanced fragmentation phenomenon which induces a loss of continuity of the carbide network, but this seems more complex since the {50h, 1100°C}–aged ***tH*** alloy presents a hardness lower than in the as–cast state despite a carbide network still script–like shaped and even coarsened. The solid solution hardening of the rather soft Ni matrix by Ta atoms, a little weakened due the decrease in Ta content in the matrix in the {50h, 1100°C}–aged state, may explain this hardness evolution.

4. Conclusion

Clearly, by replacing a part of hafnium by the equivalent quantity of tantalum, one can guess that the initial Ni–25Cr–0.4C–6Hf is probably not as performant mechanically as before. Worrisome difference in morphological stability was noticed at 1250°C (***Th*** and ***tH*** alloys) and even at 1200°C (***Th*** alloy), by comparison with the Ta–free 6Hf–containing alloy. Now, real mechanical tests at high temperature are to be scheduled to estimate the performances of these two Hf–poorest versions. In case of too large loss of resistance, other ways can be considered to correct this, as the introduction of other solid solution strengthener elements (e.g. tungsten) or directional solidification.

Acknowledgements

The authors wish to thank Lionel Aranda for his help for the thermal tests.

References

[1] S. Diliberto, C. Rapin, P. Steinmetz, P. Berthod, Microstructural and oxidation study of chromia forming molybdenum-tungsten based alloys. *Mater. Sci. Forum*, 369-372 (2001) 825-832.

[2] S. Diliberto, O. Kessler, C. Rapin, P. Steinmetz, P. Berthod, Development of chromia forming Mo-W-Cr alloys: synthesis and characterization. *J. Mater. Sci.*, 37 (2002) 3277-3284.

[3] F. Monteverde, Progress in the fabrication of ultra-high-temperature ceramics: "in situ" synthesis, microstructure and properties of a reactive hot-pressed HfB_2-SiC composite. *Composites Sci. Technol.*, 65 (2005) 1869-1879.

[4] M. Pavese, P. Fino, C. Badini, A. Ortona, G. Marino, HfB_2/SiC as a protective coating for 2D Cf/SiC composites: Effect of high temperature oxidation on mechanical properties. *Surf. Coat. Technol.*, 202 (2008) 2059-2067.

[5] X. Ren, H. Li, Y. Chu, Q. Fu, K. Li, Ultra-High-Temperature Ceramic HfB_2-SiC Coating for Oxidation Protection of SiC-Coated Carbon/Carbon Composites. *Int. J. Applied Ceram. Technol.*, 102 (2002) 2751-2772.

[6] A. Nisar, S. Bajpai, M. M. Khan, K. Balani, Wear damage tolerance and high temperature oxidation behavior of HfB_2:ZrB_2-SiC composites. *Ceram. Int.* 46 (2020) 21689-21698.

[7] R. Klein, M. Desmaison-Brut, J. Desmaison, L. Mazerolles, M. F. Trichet, High-temperature oxidation behavior of a hot isostatically-pressed Si_3N_4-HfB_2 ceramic composite. *Mater. Sci. Forum* 461-464 (2004) 849-856.

[8] D. Sciti, V. Medri, L. Silvestroni, Oxidation behavior of HfB_2-15 vol.% $TaSi_2$ at low, intermediate and high temperatures. *Scripta Materialia*, 63 (2010) 601-604.

[9] E. Opila, S. Levine, J. Lorincz, Oxidation of ZrB_2- and HfB_2-based ultra-high temperature ceramics: Effect of Ta additions. *J. Mater. Sci.*, 39 (2004) 5969-5977.

[10] E. Zapata-Solvas, D. D. Jayaseelan, H. T. Lin, P. Brown, W. E. Lee, Mechanical properties of ZrB2- and HfB2-based ultra-high temperature ceramics fabricated by spark plasma sintering. *J. Eur. Ceram. Soc.*, 33 (2013) 1373-1386.

[11] M. Gasch, S. Johnson, Physical characterization and arcjet oxidation of hafnium-based ultra high temperature ceramics fabricated by hot pressing and field-assisted sintering. *J. Eur. Ceram. Soc.*, 30 (2010) 2337-2344.

[12] S. J. Lee, E. L. Kang, S. S. Baek, D. K. Kim, Reactive hot pressing and oxidation behavior of Hf-based ultra-high-temperature ceramics. *Surf. Rev. Lett.*, 17 (2010) 215-221.

[13] C. Carney, A. Paul, S. Venugopal, T. Parthasarathy, J. Binner, A. Katz, P. Brown, Qualitative analysis of hafnium diboride based ultra high temperature ceramics under oxyacetylene torch testing at temperatures above 2100°C. *J. Eur. Ceram. Soc.*, 34 (2014) 1045-1051.

[14] S. Shimada, T. Aketo, High-temperature oxidation at 1500°C and 1600°C of SiC/graphite coated with sol-gel-derived HfO_2. *J. Am. Ceram. Soc.*, 88 (2005) 845-849.

[15] J. Sun, T. Li, A. Reitz, Q. Fu, R. Riedel, Z. Yu, High-temperature stability and oxidation behavior of SiOC/HfO_2 ceramic nanocomposite in air. *Corros. Sci.,* 175 (2020) 108866. https://doi.org/10.1016/j.corsci.2020.108866

[16] C. Musa, R. Licheri, R. Orru, G. Cao, Synthesis, Sintering, and Oxidative Behavior of HfB_2-$HfSi_2$ Ceramics. *Indus. Eng. Chem. Res.,* 53 (2014) 9101-9108.

[17] S. Wang, Y. Zhang, Y. Sun, Y. Xu, M. Yang, Synthesis and characteristic of SiBCN/HfN ceramics with high temperature oxidation resistance. *J. Alloys Compds.,* 685 (2016) 828-835.

[18] C. Young, C. Zhang, A. Loganathan, P. Nautiyal, B. Boesl, A. Agarwal, Densification and oxidation behavior of spark plasma sintered Hafnium Diboride-Hafnium Carbide composite. *Ceram. Int.*, 46 (2020) 14625-14631.

[19] Y. H. Seong, C. Baek, J. H. Kim, J. H. Kong, D. S. Kim, S. H. Lee, D. K. Kim, Evaluation of oxidation behaviors of HfC-SiC ultra-high temperature ceramics at above 2500°C via oxyacetylene torch. *Ceram. Int.*, 44 (2018) 8505-8513.

[20] H. S. Kim, B. R. Kang, S. M. Choi, Microstructure and mechanical properties of vacuum plasma sprayed HfC, TiC, and HfC/TiC ultra-high temperature ceramic coatings. *Materials*, 13 (2020) 124. https://doi.org/10.3390/ma13010124

[21] J. Cheng, J. Wang, X. Wang, H. Wang, Preparation and high-temperature performance of HfC-based nanocomposites derived from precursor with Hf-(O,N) bonds. *Ceram. Int.*, 43 (2017) 7159-7165.

[22] Q. Wen, R. Riedel, E. Ionescu, Significant improvement of the short-term high-temperature oxidation resistance of dense monolithic HfC/SiC ceramic nanocomposites upon incorporation of Ta. *Corros. Sci*,. 145 (2018) 191-198.

[23] Q. Wen, Z. Yu, R. Riedel, E. Ionescu, Significant improvement of high-temperature oxidation resistance of HfC/SiC ceramic nanocomposites with the incorporation of a small amount of boron. *J. Eur. Ceram. Soc.*, 40 (2020) 3499-3508.

[24] P. Berthod, E. Conrath, As-cast microstructures and behavior at high temperature of chromium-rich cobalt-based alloys containing hafnium carbides. *Mater. Chem. Phys.*, 140 (2014) 1139-1148.

[25] E. Conrath, P. Berthod, Kinetics of High Temperature Oxidation and Chromia Volatilization for HfC-Containing Nickel-Based Alloys. *Oxid. Met.*, 81 (2014) 393-405.

[26] P. Berthod, E. Conrath, High Temperature Oxidation of HfC-Containing Chromium-Rich Iron-Based Alloys. *Oxid. Met.*, 82 (2014) 33-48.

[27] P. Berthod, Stable Microstructural States at 1200°C of Ni–Based Alloys Containing Chromium Carbides and Tantalum Carbides. *Chem. Res. J.*, 5 (2020) 43-53.